Journal of Hazardous Materials 164 (2009) 781–789

Contents lists available at ScienceDirect

Journal of Hazardous Materials

journal homepage: www.elsevier.com/locate/jhazmat

Structural, photophysical and photocatalytic properties of novel Bi_2AlVO_7

Jingfei Luan[a,*], Wei Zhao[a], Jingwei Feng[a], Hongling Cai[b], Zheng Zheng[a], Bingcai Pan[a], Xiaoshan Wu[b], Zhigang Zou[c], Yongmei Li[d]

[a] State Key Laboratory of Pollution Control and Resource Reuse, School of the Environment, Nanjing University, Nanjing 210093, People's Republic of China
[b] National Laboratory of Solid State Microstructures, Nanjing University, Nanjing 210093, People's Republic of China
[c] Eco-Materials and Renewable Energy Research Center, Nanjing University, Nanjing 210093, People's Republic of China
[d] State Key Laboratory of Pollution Control and Resource Reuse, School of the Environment, Tongji University, Shanghai, People's Republic of China

ARTICLE INFO

Article history:
Received 23 April 2008
Received in revised form 10 August 2008
Accepted 22 August 2008
Available online 2 September 2008

Keywords:
Photocatalyst
Bi_2AlVO_7
Structural characterization
Photocatalytic degradation
Visible light irradiation

ABSTRACT

Bi_2AlVO_7 was prepared by solid-state reaction technique for the first time and the structural and photocatalytic properties of Bi_2AlVO_7 and Bi_2InTaO_7 were investigated. The results showed that Bi_2AlVO_7 crystallized in the tetragonal crystal system with space group *I*4/*mmm*. In addition, the band gaps of Bi_2AlVO_7 and Bi_2InTaO_7 were estimated to be about 2.06 and 2.81 eV. The photocatalytic degradation of aqueous methylene blue (MB) dye with Bi_2AlVO_7 or Bi_2InTaO_7 as catalyst was investigated under visible light irradiation. Bi_2AlVO_7 showed higher photocatalytic activity compared with Bi_2InTaO_7 for photocatalytic degradation of MB under visible light irradiation. Complete removal of aqueous MB dye was realized after visible light irradiation for 160 min with Bi_2AlVO_7 as the photocatalyst. The reduction of the total organic carbon (TOC) and the formation of inorganic products, SO_4^{2-} and NO_3^- revealed the continuous mineralization of aqueous MB dye during the photocatalytic process. The possible photocatalytic degradation pathway of aqueous MB dye was revealed under visible light irradiation.

1. Introduction

Since Honda and Fujishima discovered electrochemical photolysis of water at a semiconductor electrode in 1972 [1], the semiconductor photocatalysts and photocatalysis have attracted extensive attention from both academic and industrial organizations [2–10]. Up to now, some different structural photocatalysts have been produced to exploit effective utilization of solar energy [11–13]. In particular, large numbers of scientific investigations about the photocatalytic degradation of aqueous organic contaminants have been reported [14–25]. Among different contaminants, methylene blue (MB) dye is usually utilized as a probe contaminant to evaluate the activity of a photocatalyst due to the high stability against degradation in the natural environment [25–31]. However, there are only a few research findings on MB dye degradation under visible light irradiation [12,16,31–33]. Wang and Min [12] utilized nanocrystalline TiO_2/polyaniline as catalyst to photodegrade MB under natural light irradiation (λ: 190–800 nm) and found that MB could be degraded more efficiently on the TiO_2/polyaniline than on the TiO_2. Tang et al. [16] utilized $CaIn_2O_4$ as catalyst to photodegrade MB dye under visible light irradiation (λ > 420 nm) and found that MB was degraded largely after visible light irradiation, at the same time, the activity could be kept in a range of wavelength up to 580 nm. Asahi et al. [31] used films and powders of $TiO_{2-x}N_x$ as catalyst to photodegrade MB under visible light irradiation (λ < 500 nm) and found high photocatalytic reactivity. Yang et al. [32] utilized $H_3PW_{12}O_{40}/TiO_2$ as catalyst to photodegrade MB under visible light irradiation (λ > 420 nm) and found that MB could be degraded more efficiently over $H_3PW_{12}O_{40}/TiO_2$ than over TiO_2. Zhao and co-workers [33] utilized surface-fluorinated TiO_2 as catalyst to photodegrade MB under visible light irradiation (λ > 450 nm) and found that the photodegradation rate of MB was 43.1% after visible irradiation for 120 min. Therefore, it is in highly emergency to develop novel visible light-driven photocatalysts showing high activity.

Bi_2AlVO_7 is a member of the $A_2B_2O_7$ compounds, but Bi_2AlVO_7 has never been produced and the data about its structural and photophysical properties such as space group and lattice constants have not been found previously. In addition, the photocatalytic properties of Bi_2AlVO_7 have not been studied by other investigators. We consider that Al^{3+} and V^{5+} can occupy the B site and Bi^{3+} can occupy the A site in the $A_2{}^{3+}B_2{}^{4+}O_7$ compound, then an increase in hole (carrier) concentration may be realized in $Bi_2{}^{3+}Al^{3+}V^{5+}O_7$, finally a change and improvement of the electrical transportation and photophysical properties can be found in the novel $Bi_2{}^{3+}Al^{3+}V^{5+}O_7$ compound. We also confirm that Bi_2AlVO_7 may generate a slight

* Corresponding author. Tel.: +86 13 5852 06718; fax: +86 25 8370 7304.
E-mail address: jfluan@nju.edu.cn (J. Luan).

0304-3894/$ – see front matter © 2008 Elsevier B.V. All rights reserved.
doi:10.1016/j.jhazmat.2008.08.088

modification of crystal structure and cause a change in photophysical properties. Furthermore, it is proved that a slight modification of a semiconductor structure will result in a remarkable change in photocatalytic properties [16]. In this contribution, we prepared Bi_2AlVO_7 and Bi_2InTaO_7, then the structural, photophysical and photocatalytic properties of Bi_2AlVO_7 and Bi_2InTaO_7 were studied in detail. The photocatalytic properties of Bi_2AlVO_7 and Bi_2InTaO_7 were compared with that of TiO_2 (P-25) for the purpose of elucidating the structure–photocatalytic activity relationship.

2. Experimental

The novel photocatalysts were prepared by a solid-state reaction method. Al_2O_3, In_2O_3, Bi_2O_3, V_2O_5, Ta_2O_5 with purity of 99.99% (Sinopharm Group Chemical Reagent Co. Ltd., Shanghai, China) were utilized as starting materials. All powders were dried at 200 °C for 4 h before the photocatalysts were synthesized. In order to synthesize Bi_2AlVO_7, the precursors were stoichiometrically mixed, then pressed into small columns and put into an alumina crucible (Shenyang Crucible Co. Ltd., China). Finally, a calcination was carried out at 920 °C for 46 h within an electric furnace (KSL 1700X, Hefei Kejing Materials Technology CO. Ltd., China). Similarly, Bi_2InTaO_7 was synthesized by calcination at 1050 °C for 46 h. The crystal structures of Bi_2AlVO_7 and Bi_2InTaO_7 were analyzed by the powder X-ray diffraction method (D/MAX-RB, Rigaku Corporation, Japan) with Cu Kα radiation (λ = 1.54056 Å). The data were collected at 295 K with a step scan procedure θ = 5–100°. The step interval was 0.02° and the time per step was 1.2 s. The chemical compositions of the photocatalysts were examined by scanning electron microscope-X-ray energy dispersion spectrum (SEM-EDS, LEO 1530VP, LEO Corporation, Germany) and X-ray fluorescence spectrometer (XFS, ARL-9800, ARL Corporation, Switzerland). The oxygen content, Bi^{3+} content and V^{5+} content of Bi_2AlVO_7 were examined by X-ray photoelectron spectroscopy (XPS, ESCALABMK-2, VG Scientific Ltd., U.K.). The chemical composition within the depth profile of Bi_2AlVO_7 was examined by the argon ion denudation method when X-ray photoelectron spectroscopy was utilized. The optical absorption properties of Bi_2AlVO_7 and Bi_2InTaO_7 were analyzed with an UV–VIS spectrophotometer (Lambda 35, Perkin-Elmer Corporation, USA). The surface areas of the photocatalysts were measured with the BET method (MS-21, Quantachrome Instruments Corporation, USA) with N_2 adsorption at liquid nitrogen temperature. The particle sizes of the photocatalysts were measured by Malvern's Mastersize-2000 particle size analyzer (Malvern Instruments Ltd., United Kingdom).

The photocatalytic degradation of aqueous MB (Tianjin Kermel Chemical Reagent Co. Ltd.) was carried out with 0.3 g Bi_2AlVO_7 or Bi_2InTaO_7 powder suspended in 100 mL MB solution within a pyrex glass cell (Jiangsu Yancheng Huaou Industry, China). The photocatalytic reaction system consisted of a 300 W Xe arc lamp with the main emission wavelength at 436 nm (Nanjing JYZCPST Co. Ltd.), a magnetic stirrer and a cut-off filter (λ > 420 nm, Jiangsu Nantong JSOL Corporation, China). Aqueous MB solution was irradiated within a rectangular steel reactor (9 cm × 9 cm × 90 cm), equipped with a photoreactor fabricated from a quartz tube (5.8 cm in diameter and 68 cm in length). Xe arc lamp was surrounded with a quartz jacket and was positioned within the inner part of the photoreactor vessel through which a suspension of methylene blue and photocatalyst was circulated. An outer recycling water glass jacket maintained a near constant reaction temperature (22 °C), and the solution was continuously stirred and aerated. 2 mL aliquot was sampled at various time intervals. The incident photon flux I_0 measured by a radiometer (Model FZ-A, Photoelectric Instrument Factory Beijing Normal University, China) was determined to be 4.51×10^{-6} Einstein L^{-1} s^{-1} under visible light irradiation (wavelength range of 420–700 nm). The incident photon flux on the photoreactor was varied by adjusting the distance between the photoreactor and the Xe arc lamp.

The concentration of the photocatalyst was 3 g L^{-1} and the MB concentration was 0.0506 mmol L^{-1} (mol m^{-3}) with the initial pH value of 7.0. The MB concentration was examined using a UV–VIS spectrometer (Lambda 35, Perkin-Elmer Corporation, USA) with the detecting wavelength at 670 nm. The inorganic products acquired from MB degradation were detected by ion chromatograph (DX-300, Dionex Corporation, USA). The identification of MB and the degradation products was carried out by LC–MS (ThermoQuestLCQ Duo, USA) with beta basic-C_{18} HPLC column (150 × 2.1 mm i.d., 5 μm, Finnigan, Thermo, USA). 20 μL of the solution after photocatalytic reaction was injected automatically into the LC–MS system. The eluent contained 60% methanol and 40% water, and the flow rate was 0.2 mL min^{-1}. MS conditions were as follows: the electrospray ionization interface was selected. The capillary temperature was adjusted to 27 °C by a voltage of 19.00 V. The spray voltage was 5000 V and the sheath gas flow rate was 18 arb. The spectrum was obtained within the negative ion scan mode, over the m/z range from 50 to 600.

Total organic carbon (TOC) was measured with a TOC analyzer (TOC-5000, Shimadzu Corporation, Japan). The photonic efficiency was obtained according to following equation [34,35]:

$$\varphi = \frac{R}{I_0}$$

where φ is the photonic efficiency (%), R the MB degradation rate (mol L^{-1} s^{-1}), and I_0 is the incident photon flux (Einstein L^{-1} s^{-1}).

3. Results and discussion

Fig. 1(a) shows X-ray diffraction patterns of Bi_2AlVO_7 and Bi_2InTaO_7. SEM images of Bi_2AlVO_7 and Bi_2InTaO_7 are illustrated in Fig. 2(a) and (b), respectively. SEM-EDS spectrum of Bi_2AlVO_7 is illustrated in Fig. 3. The powder X-ray diffraction analysis showed that Bi_2AlVO_7 or Bi_2InTaO_7 was a single phase. It could be seen from Fig. 2 that the particle distribution of Bi_2AlVO_7 or Bi_2InTaO_7 was homogeneous and the particle morphology was regular. The average particle size of Bi_2AlVO_7 or Bi_2InTaO_7 was measured to be 1.5 or 1.2 μm by using Malvern's Mastersize-2000 particle size analyzer. Furthermore, it also could be seen from Fig. 2(a) that Bi_2AlVO_7 possessed high crystallinity and characteristic lamellar lumpish crystal structure, which probably resulted in a decrease for the migration distance of photogenerated electrons and holes to reach the reaction site on the surface, then the creation of active sites was realized [36]. As a result, it would probably improve the photocatalytic activities. The chemical composition of the compound was examined by using characteristic X-rays of Bi M, Bi L, V K, Al K and O K with the ZAF (element number, absorption and fluorescence corrections) quantification method. The SEM-EDS analysis revealed that Bi_2AlVO_7 had a homogenous atomic distribution without other impure elements. Fig. 4 shows the XPS spectrum of Bi^{3+} coming from Bi_2AlVO_7. An average atomic ratio of Bi:Al:V:O = 2.00:0.98:1.02:6.98 for Bi_2AlVO_7 was acquired according to XPS, SEM-EDS and XFS analysis. In addition, XRD results also showed that Bi_2AlVO_7 was a single phase. According to XPS analysis, the oxidation state of Bi, Al, V, and O ion is +3, +3, +5 and −2, respectively. Based on above analysis, it could be concluded that the chemical formula of the novel compound was $Bi_{2.00}{}^{3+}Al_{0.98}{}^{3+}V_{1.02}{}^{5+}O_{6.98}{}^{2-}$ (predigested as Bi_2AlVO_7). According to above results, we could conclude that the resulting materials are of high purity under our preparation conditions.

Full-profile structure refinement of the collected powder diffraction data for Bi_2AlVO_7 and Bi_2InTaO_7 was performed with

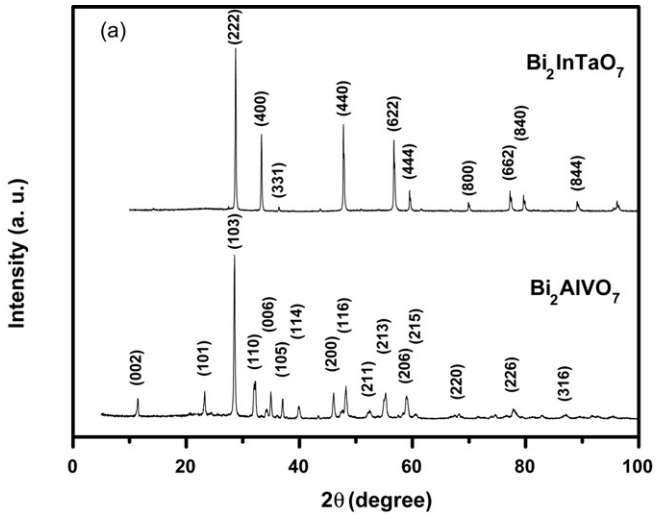

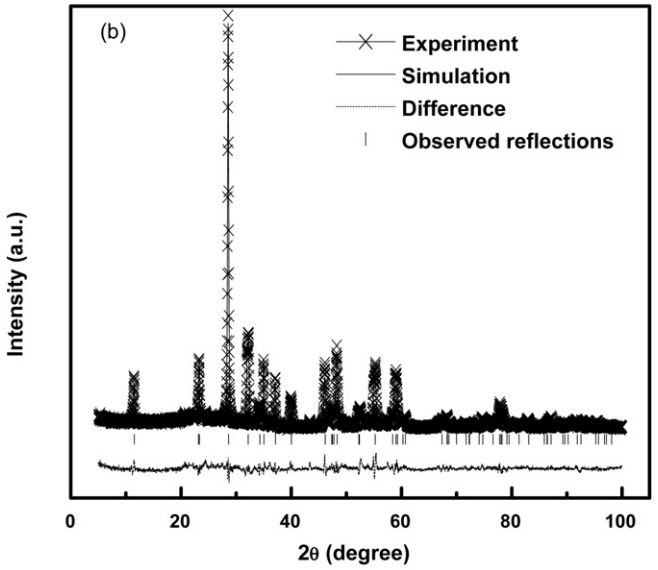

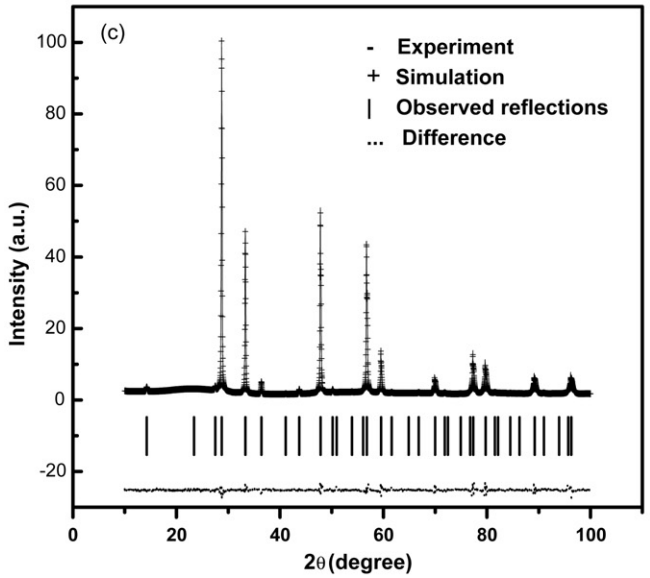

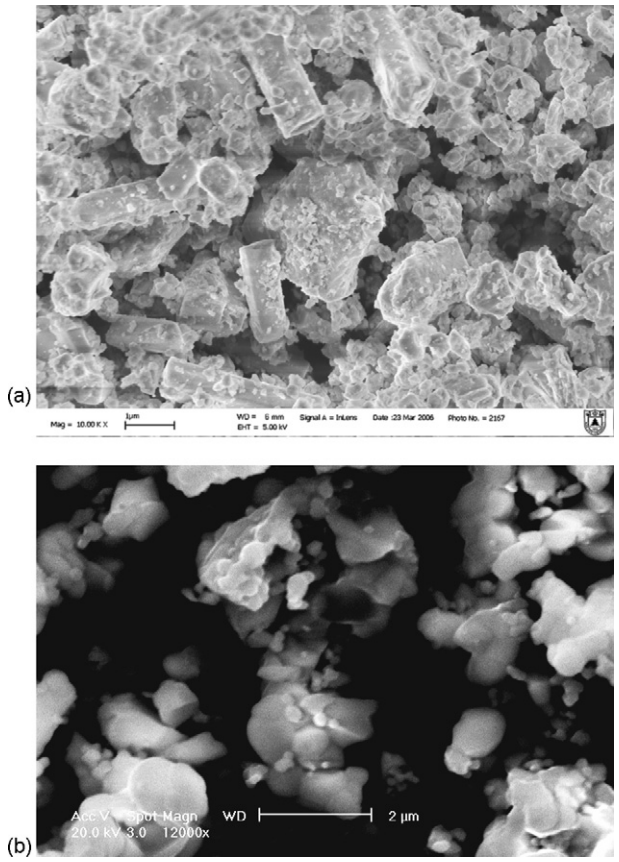

Fig. 2. SEM images of Bi_2AlVO_7 and Bi_2InTaO_7. (a) Bi_2AlVO_7, (b) Bi_2InTaO_7.

the Rietveld program REITAN [37], by which positional parameters of Bi_2AlVO_7 and Bi_2InTaO_7 were refined. The refinement results of Bi_2AlVO_7 and Bi_2InTaO_7 are shown in Fig. 1(b) and (c). The atomic coordinates and structural parameters of Bi_2AlVO_7 and Bi_2InTaO_7 are indicated in Tables 1 and 2. The result of the final refinement for Bi_2AlVO_7 confirmed a good agreement between the observed intensities and calculated intensities for the tetragonal crystal system with space group $I4/mmm$ when the O atoms are included in the model. The lattice parameters of Bi_2AlVO_7 were found to be $a = 3.9294(1)$, $b = 3.9294(1)$, $c = 15.3469(9)$ Å. All the diffraction peaks of Bi_2AlVO_7 could be successfully indexed according to above lattice constant and space group. The final refinement result of Bi_2InTaO_7 generated the unweighted and weighted R factors, $R_P = 11.16\%$, $R_{WP} = 14.91\%$ with the pyrochlore type crystal structure, cubic system and space group $Fd3m$ when the O atoms are included in the model, as a result, the lattice parameter of Bi_2InTaO_7 is obtained to be $a = 10.7464(1)$ Å. Our X-ray diffraction results indicated that Bi_2AlVO_7 and Bi_2InTaO_7 crystallized with different structures. The cubic system structure with space group $Fd3m$ for Bi_2InTaO_7 were changed into tetragonal system structure with space group $I4/mmm$ by using Ta^{5+} being substituted by V^{5+} and In^{3+} being substituted by Al^{3+}. The refinement results of Bi_2AlVO_7 generated the unweighted R factor, $R_P = 12.9\%$ with space group $I4/mmm$.

Fig. 1. (a) X-ray powder diffraction patterns of Bi_2AlVO_7 and Bi_2InTaO_7. (b) Rietveld refinement results of XRD data for Bi_2AlVO_7 by a solid-state reaction method at 920 °C. A difference (observed – calculated) profile is shown beneath. The tic marks represent reflection positions. (c) Rietveld refinement results of XRD data for Bi_2InTaO_7 by a solid-state reaction method at 1050 °C. A difference (observed – calculated) profile is shown beneath. The tic marks represent reflection positions.

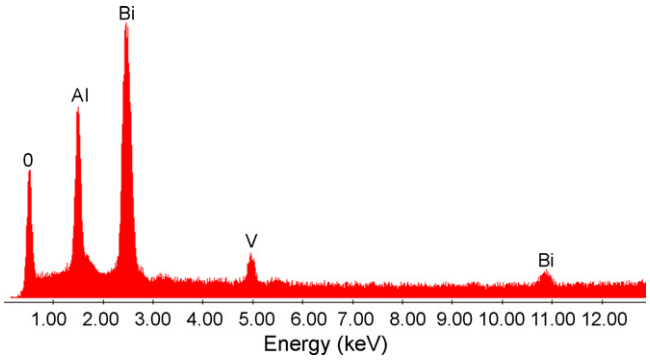

Fig. 3. SEM-EDS spectrum taken from Bi_2AlVO_7.

Zou et al. [4] refined the crystal structure of Bi_2InNbO_7 and acquired a large *R* factor for Bi_2InNbO_7, which was owing to a slightly modified structure model from Bi_2InNbO_7. The high pure precursors were used in this study, thus the effect of minor impurities on the structure of Bi_2AlVO_7 or Bi_2InTaO_7 could be excluded, which was further supported by the experimental results that impurities were not detected by EDS analysis. Therefore, we supposed that the slight high *R* factor for Bi_2AlVO_7 was derived from a slightly modified structure model for Bi_2AlVO_7. It should be emphasized that the defects, disorder or order of partial atoms could result in the change of structures, including different bond-distance distributions, thermal displacement parameters or occupation factors for some of the atoms.

Fig. 5 shows the results of diffuse reflection spectra of Bi_2AlVO_7 and Bi_2InTaO_7. For Bi_2AlVO_7, an average absorption of less than 18.0% was obtained from 600 to 800 nm. For Bi_2InTaO_7, an average absorption of less than 1.2% was acquired from 500 to 800 nm. In contrast to the well-known TiO_2 which showed absorption edge at about 400 nm, the novel synthesized Bi_2AlVO_7 exhibited obvious absorption in visible light region up to 598 nm, which made clear that Bi_2AlVO_7 had the ability to respond to visible light. For a crystalline semiconductor compound, it is known that the optical absorption near the band edge of semiconductor compound follows the equation [38,39]: $\alpha h\nu = A(h\nu - E_g)^n$. *A*, α, E_g and ν are proportional constant, absorption coefficient, band gap and light frequency, respectively. Fig. 6 shows the Plot of $(\alpha h\nu)^{1/n}$ versus $h\nu$ for Bi_2AlVO_7 and Bi_2InTaO_7. It could be seen from Fig. 6 that the band gaps of Bi_2AlVO_7 and Bi_2InTaO_7 were calculated to be 2.06 and 2.81 eV, indicating that Bi_2AlVO_7 possessed narrower band gap compared with that of Bi_2InTaO_7. This may imply that the photoabsorption of Bi_2AlVO_7 is stronger than that of Bi_2InTaO_7, which may cause a higher photocatalytic activity of Bi_2AlVO_7 than that of Bi_2InTaO_7. Usually, the photoabsorption of the photocatalyst depends on the mobility ability of electron-hole pairs, which determines the probability of electrons and holes to reach reaction sites of the photocatalyst surface.

Table 1
Structural parameters of Bi_2AlVO_7 prepared by solid-state reaction method

Atom	*x*	*y*	*z*	Occupation factor
Bi	0.0000	0.5000	0.2500	1.0
Al	0.0000	0.5000	0.0000	0.5
V	0.0000	0.5000	0.0000	0.5
O(1)	0.0000	0.0000	0.0000	1.0
O(2)	0.0000	0.0000	0.3317	1.0
O(3)	−0.2558	0.5000	0.0000	1.0

Table 2
Structural parameters of Bi_2InTaO_7 prepared by solid-state reaction method

Atom	*x*	*y*	*z*	Occupation factor
Bi	0.0000	0.0000	0.0000	1.0
In	0.5000	0.5000	0.5000	0.5
Ta	0.5000	0.5000	0.5000	0.5
O(1)	−0.1862	0.1250	0.1250	1.0
O(2)	0.1250	0.1250	0.1250	1.0

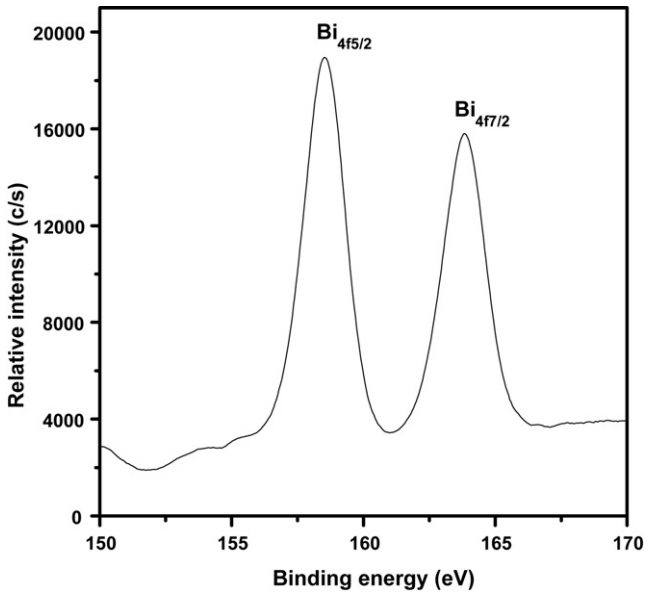

Fig. 4. XPS spectrum of Bi^{3+} derived from Bi_2AlVO_7.

MB degradation with Bi_2AlVO_7, Bi_2InTaO_7 or TiO_2 as the photocatalyst under visible light irradiation ($\lambda > 420$ nm) within oxygen-saturated suspension ($[O_2]_{sat} = 1.02 \times 10^{-3}$ M), is shown in Fig. 7. By means of Bi_2AlVO_7, the results indicated that the solution color changed from deep blue to colorless and MB concentration within the solution decreased to 0 mol m^{-3} after visible light irradiation for 160 min. The initial rate of MB degradation was 5.27×10^{-6} mol s^{-1} m^{-3}. At the same time, a SO_4^{2-} ion concentration of 0.0329 mol m^{-3} and a NO_3^- ion concentration of 0.1518 mol m^{-3} were detected within the solution after the photocatalytic reaction for 160 min, indicating that 65% of sulfur coming

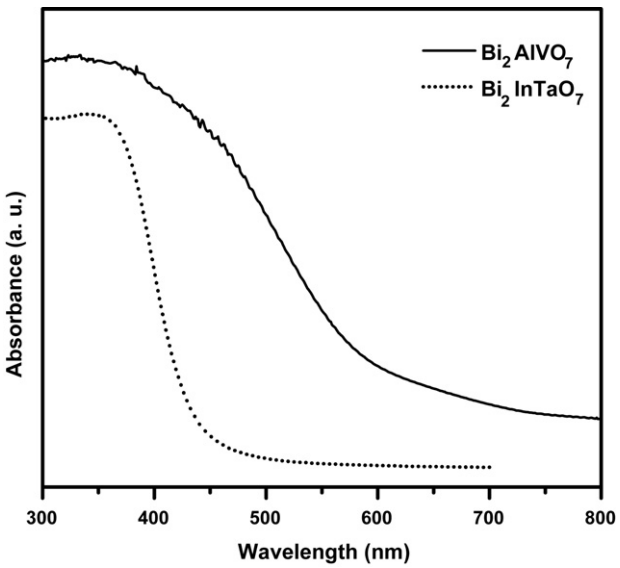

Fig. 5. Diffuse reflection spectra of Bi_2AlVO_7 and Bi_2InTaO_7 prepared by a solid-state reaction method.

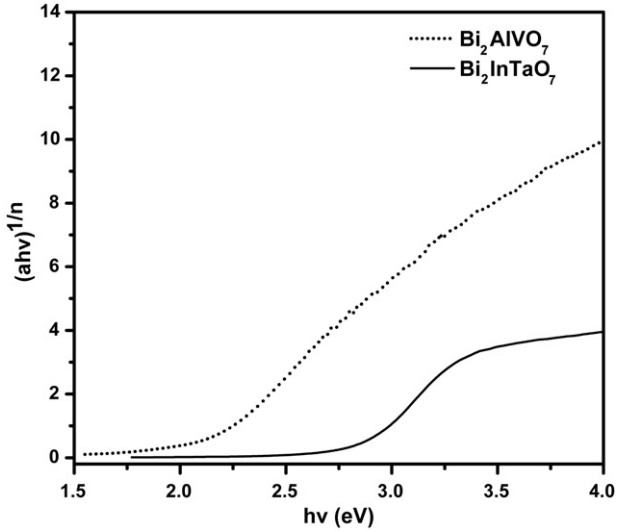

Fig. 6. Plot of $(\alpha h\nu)^{1/n}$ versus $h\nu$ for Bi_2AlVO_7 and Bi_2InTaO_7.

from MB was turned into sulfate ion. By identifying the photodegradation intermediates of MB in our experiment, we found that the photodegradation intermediates were azure B, azure A, thionine, phenothiazine, leucomethylene blue, *N*,*N*-dimethyl-*p*-phenylenediamine, benzenesulfonic acid, phenol and aniline. Based on the intermediate products found in this work, a possible photocatalytic degradation pathway of MB is proposed in Fig. 8. The methyl groups were turned into smaller organic species and ultimately were mineralized to inorganic products such as CO_2, NH_4^+, NO_3^- and SO_4^{2-}. The sulfur was hydrolytically removed first, then the sulfur was subsequently oxidized and transformed into SO_4^{2-}, at the same time, nitrogen atoms with −3 oxidation state produced NH_4^+ cations, subsequently NH_4^+ cations were converted into NO_3^- ions. It was clear that aqueous MB was mainly mineralized rather than being bleached under our experimental conditions owing to the decrease of the TOC (100%) after 160 min irradiation. Hidaka and co-workers [29] decomposed MB with TiO_2 as catalyst under UV illumination and they found that the photocatalytic degradation pathway of MB was as following intermediates order: azure B, azure A, azure C, thionine and phenothiazine. It is obvious that the photocatalytic degradation pathway of MB was similar between their results [29] and our results. The difference of the photocatalytic degradation pathway of MB was that we did not find azure C but we found leucomethylene blue, benzenesulfonic acid and *N*,*N*-dimethyl-*p*-phenylenediamine. Herrmann and co-workers [30] also investigated the TiO_2/UV photocatalytic degradation pathway of MB and they found that the photodegradation intermediates of MB were mainly aromatic metabolites such as phenothiazine, hydroxyhydroquinone, benzenesulfonic acid and phenol. They [30] considered that the initial step of MB degradation was ascribed to the cleavage of the bonds of the C–S^+=C functional group within MB. The photocatalytic degradation pathway of MB accomplished by Herrmann and co-workers [30] and us was also similar because we achieved some consilient photodegradation intermediates of MB such as phenothiazine, benzenesulfonic acid and phenol. However, the difference of the photocatalytic degradation pathway of MB was that we did not find hydroxyhydroquinone but we found leucomethylene blue, azure B, azure A and thionine.

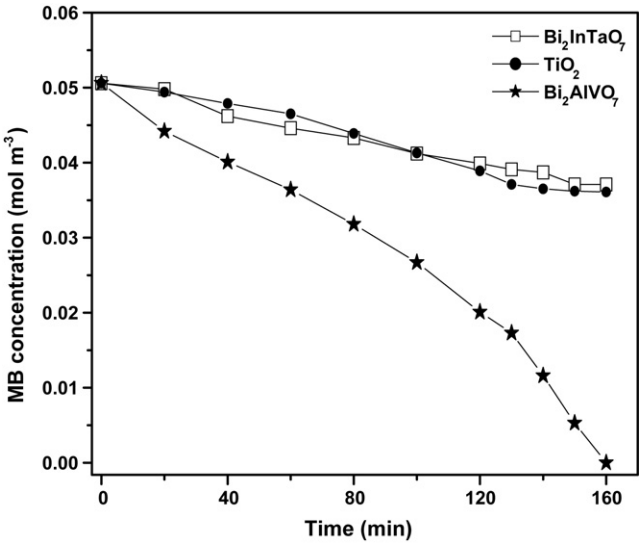

Fig. 7. Photocatalytic methylene blue degradation under visible light irradiation ($\lambda > 420$ nm) within oxygen-saturated suspension ($[O_2]_{sat} = 1.02 \times 10^{-3}$ M) by the existence of Bi_2AlVO_7 and Bi_2InTaO_7, as well as TiO_2.

The initial photonic efficiency was calculated to be 0.117% for Bi_2AlVO_7. However, with Bi_2InTaO_7 as the catalyst, aqueous MB concentration decreased only from 0.0506 to 0.0371 mol m^{-3} after visible light irradiation for 160 min and the initial rate of MB degradation was 1.41×10^{-6} mol s^{-1} m^{-3}. The initial photonic efficiency was calculated to be 0.031% for Bi_2InTaO_7. Simultaneously, a SO_4^{2-} ion concentration of 0.0090 mol m^{-3} and a NO_3^- ion concentration of 0.0405 mol m^{-3} were detected within the solution after the photocatalytic reaction for 160 min, indicating that 67% of sulfur derived from MB was turned into sulfate ion. The result showed that the rate of MB degradation with Bi_2AlVO_7 as the catalyst was higher than MB degradation rate with Bi_2InTaO_7 as the catalyst, indicating that Bi_2AlVO_7 was more active for MB photocatalytic degradation under visible light irradiation compared with Bi_2InTaO_7. The surface areas of Bi_2AlVO_7 and Bi_2InTaO_7 were 1.14 and 1.26 m^2 g^{-1}, respectively. This clearly proved that the higher photocatalytic activity of Bi_2AlVO_7 was not attributed to the large surface area.

By means of TiO_2, visible light irradiation for 160 min caused the decrease of MB concentration from 0.0506 to 0.0361 mol m^{-3}. The initial rate of MB degradation and the photonic efficiency were 1.51×10^{-6} mol s^{-1} m^{-3} and 0.033%. In addition, SO_4^{2-} ion was not detected within the solution after the photoreaction. The results indicated that MB degradation rate with Bi_2InTaO_7 as the catalyst was almost identical to MB degradation rate with TiO_2 as the catalyst, indicating that TiO_2 was inactive for MB photocatalytic degradation under visible light irradiation.

One of the photocatalytic degradation mechanism of MB under visible light irradiation was as follows: the direct absorption of photons by Bi_2AlVO_7 resulted in the generation of excited electrons within the conduction band and photogenerated holes within the valence band of Bi_2AlVO_7. The excited electrons within the conduction band of Bi_2AlVO_7 could be captured by surface sorbed O_2, which eventually suppressed the recombination of photogenerated electrons and photogenerated holes. As a result, the photogenerated holes within the valence band of Bi_2AlVO_7 could serve as the oxidizing species for inducing MB photodegradation.

Another two possible degradation mechanisms of MB with Bi_2AlVO_7 or TiO_2 as photocatalyst were proposed as follows: for photocatalytic degradation of MB with Bi_2AlVO_7 as catalyst under visible light irradiation, the initial process of MB degradation could be described by Scheme I (Eqs. (1)–(3)) and Scheme II (Eqs. (4)–(6)). For photocatalytic degradation of MB with TiO_2 as catalyst under visible light irradiation, the initial process of MB degradation could not be described by Scheme III (Eqs. (7)–(9)) but could be described

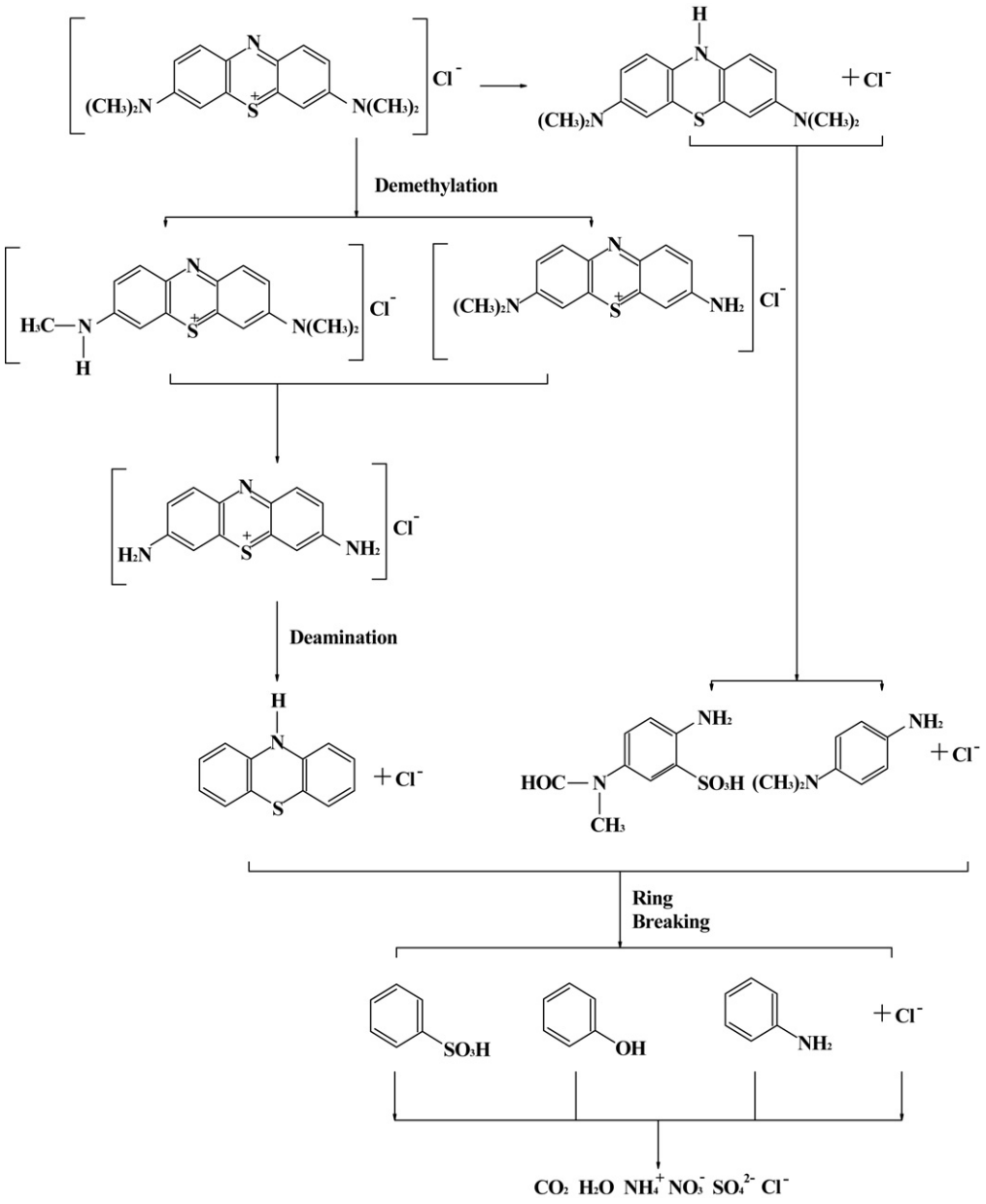

Fig. 8. Possible photocatalytic degradation pathway scheme of MB.

by Scheme IV (Eqs. (10)–(12)). As shown in Schemes I and III, the generated hydroxy radicals could further oxidize the pollutant MB. As shown in Schemes II and IV, a photosensitization process with MB as a sensitizer was realized, and the degradation mechanism of MB in this process could be described by Schemes II and IV, in which MB adsorbed on Bi_2AlVO_7 or TiO_2 was excited by visible light irradiation and then an electron was injected from the excited MB to the conduction band of Bi_2AlVO_7 or TiO_2 where the electron was scavenged by molecular oxygen [17].

Scheme I:

$$Bi_2AlVO_7 \xrightarrow{\text{visible light}} h^+ + e^- \quad (1)$$

$$e^- + O_2 \rightarrow {}^{\bullet}O_2^- \quad (2)$$

$$h^+ + OH^- \rightarrow {}^{\bullet}OH \quad (3)$$

Scheme II:

$$MB_{(ads)} \xrightarrow{\text{visible light}} MB^*_{(ads)} \quad (4)$$

$$MB^*_{(ads)} + Bi_2AlVO_7 \rightarrow Bi_2AlVO_7(e) + MB^+_{(ads)} \quad (5)$$

$$Bi_2AlVO_7(e) + O_2 \rightarrow Bi_2AlVO_7 + {}^{\bullet}O_2^- \quad (6)$$

Scheme III:

$$TiO_2 \xrightarrow{\text{ultraviolet light}} h^+ + e^- \quad (7)$$

$$e^- + O_2 \rightarrow {}^{\bullet}O_2^- \quad (8)$$

$$h^+ + OH^- \rightarrow {}^{\bullet}OH \quad (9)$$

Scheme IV:

$$MB_{(ads)} \xrightarrow{\text{visible light or ultraviolet light}} MB^*_{(ads)} \quad (10)$$

$$MB^*_{(ads)} + TiO_2 \rightarrow TiO_2(e) + MB^+_{(ads)} \quad (11)$$

$$TiO_2(e) + O_2 \rightarrow TiO_2 + {}^{\bullet}O_2^- \quad (12)$$

After visible light irradiation for 120 min with TiO_2 as catalyst, approximately 28.2% and 23.1% of MB were degraded by Tang et al. [16] and Luan et al. respectively, indicating that their degradation efficiencies of MB were similar. The reason that the degradation rate of MB by Luan et al. was a little lower than that by Tang et al. [16] was mainly as follows: the initial MB concentration of 0.0506 mol m^{-3} utilized by Luan et al. was a little higher than the initial MB concentration of 0.0478 mol m^{-3} used by Tang, as a result, the low capacity of visible light irradiation to penetrate through a media that contained higher concentration of MB resulted in a decrease of MB degradation rate. Tang et al. [16] also concluded that the possible degradation mechanism of MB over TiO_2 was only based on dye-sensitized process under visible light irradiation. Zhao et al. [40] also reported that alizarin red and X3B dyes could be degraded over TiO_2 based on visible light driven dye-sensitized mechanism. Thus, the photocatalytic degradation of MB over TiO_2 in our experiment was also based on dye-sensitized process (see Scheme IV, Eqs. (10)–(12)). Under the condition of visible light irradiation, the photocatalytic degradation of MB over TiO_2 in our experiment or in Tang's experiment [16] was impossible to be derived from Scheme III (Eqs. (7)–(9)).

In addition, after visible light irradiation for 120 min with Bi_2AlVO_7 as catalyst, approximately 60.3% of MB was degraded by us, indicating that the degradation efficiency of MB with Bi_2AlVO_7 as catalyst was much higher than that obtained from Tang et al. [16] or Luan et al. with TiO_2 as catalyst, and the reason was mainly as follows: the degradation mechanisms of MB with Bi_2AlVO_7 as catalyst under visible light irradiation was Scheme I (Eqs. (1)–(3)) and Scheme II (Eqs. (4)–(6)), but the degradation mechanisms of MB with TiO_2 as catalyst under visible light irradiation was only Scheme IV (Eqs. (10)–(12)). Based on above analysis, Bi_2AlVO_7 was also more active for MB photocatalytic degradation under visible light irradiation compared with TiO_2.

The final photodegradation goal of organic pollutants is to completely change the toxic organic compounds into inorganics, such as CO_2, SO_4^{2-} or NO_3^-, etc. With the existence of Bi_2AlVO_7 or Bi_2InTaO_7, the dependence of MB degradation products on the irradiation time is indicated in Fig. 9. It could be seen that the concentration of SO_4^{2-} or NO_3^- ions increased obviously with increasing irradiation time. The stoichiometry amount of SO_4^{2-} is also shown in Fig. 9, indicating that the amount of SO_4^{2-} ions released into the solution was lower than that expected from stoichiometry amount of SO_4^{2-}. The first possible reason was the loss of sulfur-containing volatile compounds such as SO_2. The second probable reason was shown by the partially irreversible adsorption of some SO_4^{2-} ions on the surface of the photocatalyst as already observed by Lachheb et al. [28]. However, the partial irreversible adsorption of SO_4^{2-} ions did not suppress the photocatalytic degradation of pollutants. The higher amount of NO_3^- ions was due to the stoichiometric ratio $N/S = 3$ within the initial MB molecule.

The TOC removal of MB during visible light irradiation is shown in Fig. 10. The results showed that 100% or 23.60% of TOC decrease was obtained after visible light irradiation for 160 min with Bi_2AlVO_7 or Bi_2InTaO_7 as the photocatalyst. Based on above analysis, the complete mineralization of MB with Bi_2AlVO_7 as the photocatalyst was achieved after 160 min irradiation due to the decrease of the TOC (100%).

The research concerning the luminescent properties had drawn a conclusion that the closer the M–O–M bond angle was to 180°, the more the excited state was delocalized [41]. This indicates that the photoinduced electrons and holes can move easily if the M–O–M bond angle is close to 180°. The mobility ability of the photoinduced electrons and holes also affects the photocatalytic activity because

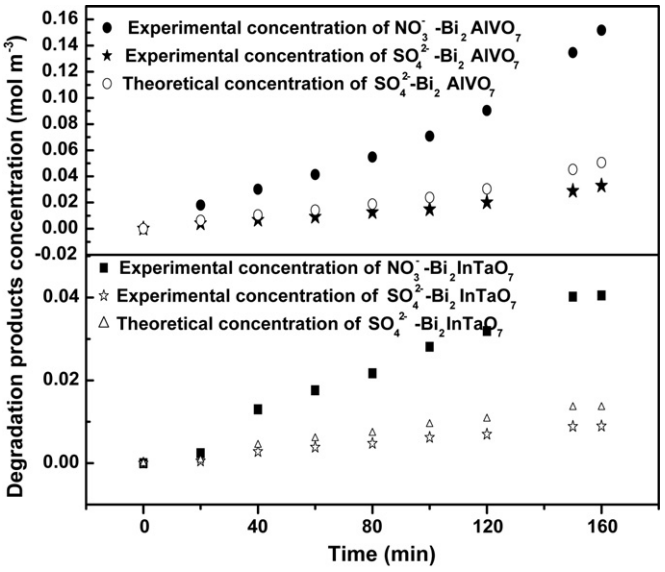

Fig. 9. Evolution of SO_4^{2-} and NO_3^- ions in the solution with Bi_2AlVO_7 or Bi_2InTaO_7 as photocatalyst during the photocatalytic degradation of MB under visible light irradiation ($\lambda > 420$ nm) within oxygen-saturated suspension ($[O_2]_{sat} = 1.02 \times 10^{-3}$ M).

the mobility ability affects the probability of electrons and holes to reach reaction sites onto the catalyst surface. In this experiment, the Al–O–V bond angle was nearly 180° and the photocatalytic activities of Bi_2AlVO_7 were accordingly higher. The crystal structures of Bi_2AlVO_7 and Bi_2InTaO_7 are different, and their electronic structures are also considered to be different. For Bi_2AlVO_7, V is 3d-block metal element, and for Bi_2InTaO_7, Ta is 5d-block metal element, indicating that the photocatalytic activity may be influenced not only by the crystal structure but also by the electronic structure of the photocatalyst. Based on above analysis, the differences of photocatalytic degradation efficiency of MB between Bi_2AlVO_7 and Bi_2InTaO_7 were mainly due to the differences of their crystal structure and electronic structure. Fig. 11 shows the suggested band structures of Bi_2AlVO_7 and Bi_2InTaO_7. Recently, the electronic structures of $InMO_4$ (M = V, Nb and Ta) and $BiVO_4$ were reported by

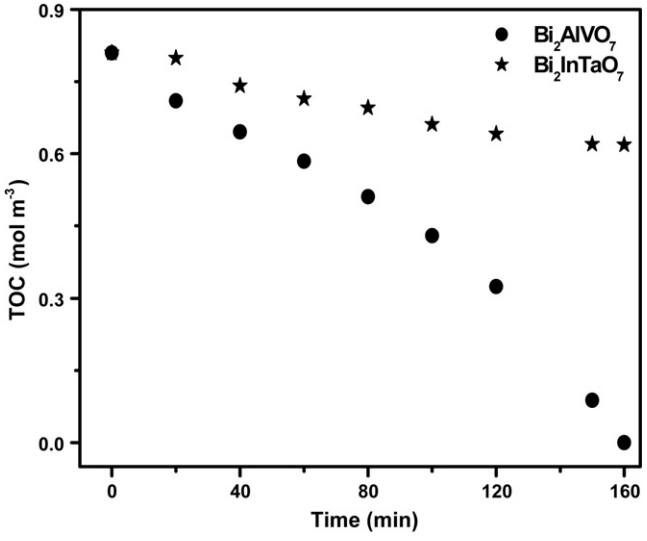

Fig. 10. Disappearance of total organic carbon (TOC) during the photocatalytic degradation of MB with Bi_2AlVO_7 or Bi_2InTaO_7 as photocatalyst under visible light irradiation ($\lambda > 420$ nm) within oxygen-saturated suspension ($[O_2]_{sat} = 1.02 \times 10^{-3}$ M).

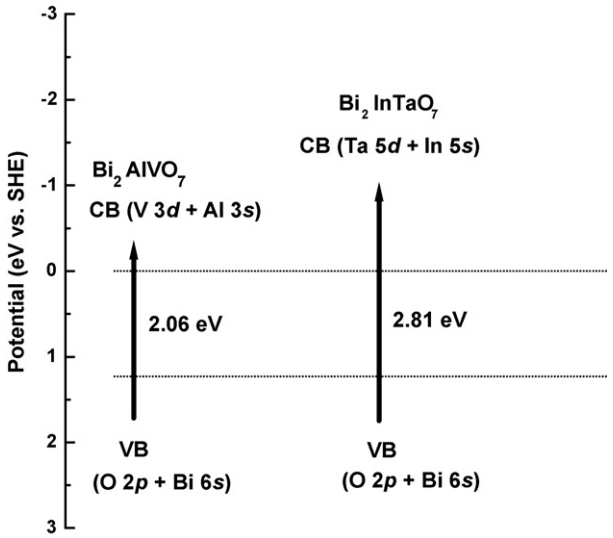

Fig. 11. Suggested band structures of Bi_2AlVO_7 and Bi_2InTaO_7.

Oshikiri et al. according to the first principle calculations [42]. The conduction bands of $InMO_4$ (M = V, Nb and Ta) mainly contained a dominant d orbital component from V 3d, Nb 4d and Ta 5d orbitals, respectively. The valence bands of $BiVO_4$ mainly contained a small Bi 6s orbital component and a dominant O 2p orbital component. The band structures of Bi_2AlVO_7 and Bi_2InTaO_7 should be similar to those of $InMO_4$ (M = V, Nb and Ta) and $BiVO_4$. Therefore, we concluded that the conduction band of Bi_2AlVO_7 mainly contained V 3d and Al 3s. The valence band of Bi_2AlVO_7 mainly contained a small Bi 6s orbital component and a dominant O 2p orbital component. Similarly, the conduction band of Bi_2InTaO_7 mainly contained Ta 5d and In 5s. The valence band of Bi_2InTaO_7 mainly contained a small Bi 6s orbital component and a dominant O 2p orbital component. Direct absorption of photons by Bi_2AlVO_7 can produce electron–hole pairs within the catalyst, indicating that the larger energy than the band gap of Bi_2AlVO_7 is necessary for degrading MB by photocatalysis.

Above results indicated that Bi_2AlVO_7/(visible light) photocatalysis might be regarded as a method for practical treatment of diluted colored waste water. Our Bi_2AlVO_7/(visible light) photocatalysis system can be utilized for decolorization, purification and detoxification in textile industries, printing and dyeing industries in semi-arid countries such as South Africa. We designed Bi_2AlVO_7/(visible light) photocatalysis system without demanding chemical reagents or using high pressure of oxygen or heating. The decolorized and detoxified water were submitted to our new system for treatment and the results showed that the Bi_2AlVO_7/(visible light) photocatalysis system might provide a valuable treatment for purifying and reusing colored aqueous effluents. A part of our work has been done in Wuxi city which is rich both in textile industries and in solar energy. Practical experiments with waste water treatment pilot plant were found inspiring.

4. Conclusions

We synthesized single phase of Bi_2AlVO_7 or Bi_2InTaO_7 by solid-state reaction method and studied the structural, photophysical and photocatalytic properties of Bi_2AlVO_7 and Bi_2InTaO_7. XRD results showed that Bi_2AlVO_7 crystallized with the tetragonal crystal system and space group $I4/mmm$. Bi_2InTaO_7 crystallized with the pyrochlore type crystal structure, cubic system and space group $Fd3m$. The lattice parameters of Bi_2AlVO_7 were found to be $a = b = 3.9294(1)$, $c = 15.3469(9)$ Å. The lattice parameter of Bi_2InTaO_7 was found to be $a = 10.7464(1)$ Å. The band gaps of Bi_2AlVO_7 and Bi_2InTaO_7 were calculated to be about 2.06 and 2.81 eV and Bi_2AlVO_7 showed strong optical absorption within the visible light region ($\lambda > 420$ nm). With the existence of Bi_2AlVO_7, photocatalytic degradation of aqueous MB could be obtained under visible light irradiation. Simultaneously, the mineralization of aqueous MB resulted in the generation of SO_4^{2-} and NO_3^- ions and resulted in the remarkable decrease of TOC during the reaction, which indicated that Bi_2AlVO_7/(visible light) system might be regarded as an effective method for treatment of the wastewater from the textile industries, printing and dyeing industries. The photodegradation intermediates of MB were identified and the possible photocatalytic degradation pathway of MB was revealed under visible light irradiation.

Acknowledgement

This work was supported by the National Natural Science Foundation of China (No.20877040) and by a grant from the Natural Science Foundation of Jiangsu Province (No. BK2007717, BK2006130).

References

[1] K. Honda, A. Fujishima, Electrochemical photolysis of water at a semiconductor electrode, Nature 238 (1972) 37–38.
[2] M. Kitano, M. Takeuchi, M. Matsuoka, J.M. Thomas, M. Anpo, Preparation of visible light-responsive TiO_2 thin film photocatalysts by an RF magnetron sputtering deposition method and their photocatalytic reactivity, Chemistry Letters 34 (4) (2005) 616–617.
[3] B. Neppolian, H. Yamashita, Y. Okada, H. Nishijima, M. Anpo, Preparation of unique TiO_2 nano-particle photocatalysts by a multi-gelation method for control of the physicochemical parameters and reactivity, Catalysis Letters 105 (1–2) (2005) 111–117.
[4] Z.G. Zou, J.H. Ye, H. Arakawa, Preparation, structural and photophysical properties of Bi_2InNbO_7 compound, Journal of Materials Science Letters 19 (2000) 1909–1911.
[5] Z.G. Zou, J.H. Ye, K. Sayama, H. Arakawa, Direct splitting of water under visible light irradiation with an oxide semiconductor, Nature 414 (2001) 625–627.
[6] Y.V. Meteleva, F. Roessner, G.F. Novikov, Synthesis and optical properties of zeolite–semiconductor composites—new photocatalysts, Journal of Photochemistry and Photobiology A: Chemistry 196 (2–3) (2008) 154–158.
[7] J.H. Tay, X.G. Chen, S. Jeyaseelan, N. Graham, Optimising the preparation of activated carbon from digested sewage sludge and coconut husk, Chemosphere 44 (1) (2001) 45–51.
[8] L. Ge, Synthesis and characterization of novel visible-light-driven Pd/$BiVO_4$ composite photocatalysts, Materials Letters 62 (6–7) (2008) 926–928.
[9] B. Neppolian, Q.L. Wang, H. Yamashita, H. Choi, Synthesis and characterization of ZrO_2–TiO_2 binary oxide semiconductor nanoparticles: application and interparticle electron transfer process, Applied Catalysis A: General 333 (2) (2007) 264–271.
[10] A. Dodd, A. McKinley, T. Tsuzuki, M. Saunders, Optical and photocatalytic properties of nanocrystalline TiO_2 synthesised by solid-state chemical reaction, Journal of Physics and Chemistry of Solids 68 (12) (2007) 2341–2348.
[11] R.S. Sonawane, M.K. Dongare, Sol-gel synthesis of Au/TiO_2 thin films for photocatalytic degradation of phenol in sunlight, Journal of Molecular Catalysis A-Chemical 243 (1) (2006) 68–76.
[12] F. Wang, S.X. Min, TiO_2/polyaniline composites: an efficient photocatalyst for the degradation of methylene blue under natural light, Chinese Chemical Letters 18 (10) (2007) 1273–1277.
[13] H.B. Fu, C.S. Pan, W.Q. Yao, Y.F. Zhu, Visible-light-induced degradation of rhodamine B by nanosized Bi_2WO_6, Journal of Physical Chemistry B 109 (47) (2005) 22432–22439.
[14] D. Fabbri, A.B. Prevot, V. Zelano, M. Ginepro, E. Pramauro, Removal and degradation of aromatic compounds from a highly polluted site by coupling soil washing with photocatalysis, Chemosphere 71 (1) (2008) 59–65.
[15] C. Kim, S.J. Doh, S.G. Lee, S.J. Lee, H.Y. Kim, Visible-light absorptivity of a zincoxysulfide (ZnO_xS_{1-x}) composite semiconductor and its photocatalytic activities for degradation of organic pollutants under visible-light irradiation, Applied Catalysis A: General 330 (2007) 127–133.
[16] J.W. Tang, Z.G. Zou, J. Yin, J.H. Ye, Photocatalytic degradation of methylene blue dye on $CaIn_2O_4$ under visible light irradiation, Chemical Physics Letters 382 (2003) 175–179.
[17] C. Nasr, K. Vinodgopal, L. Fisher, S. Hotchandani, A.K. Chattopadhyay, P.V. Kamat, Environmental photochemistry on semiconductor surfaces-visible light induced degradation of a textile diazo dye, naphthol blue black, on TiO_2 nanoparticles, Journal of Physical Chemistry 100 (1996) 8436–8442.

[18] J.H. Tay, P. Yang, W.Q. Zhuang, S.T.L. Tay, Z.H. Pan, Reactor performance and membrane filtration in aerobic granular sludge membrane bioreactor, Journal of Membrane Science 304 (1–2) (2007) 24–32.
[19] D. Chatterjee, S. Dasgupta, Visible light induced photocatalytic degradation of organic pollutants, Journal of Photochemistry and Photobiology C-Photochemistry Reviews 6 (2–3) (2005) 186–205.
[20] G. Granados, C.A. Paez, F. Martinez, E.A. Paez-Mozo, Photocatalytic degradation of phenol on TiO_2 and TiO_2/Pt sensitized with metallophthalocyanines, Catalysis Today 107 (2005) 589–594.
[21] J.W. Tang, J.H. Ye, Photocatalytic and photophysical properties of visible-light-driven photocatalyst $ZnBi_{12}O_{20}$, Chemical Physics Letters 410 (1–3) (2005) 104–107.
[22] M.M. Haque, M. Muneer, D.W. Bahnemann, Semiconductor-mediated photocatalyzed degradation of a herbicide derivative, chlorotoluron, in aqueous suspensions, Environmental Science & Technology 40 (15) (2006) 4765–4770.
[23] J. Marugan, D. Hufschmidt, M.J. Lopez-Munoz, V. Selzer, D.W. Bahnemann, Photonic efficiency for methanol photooxidation and hydroxyl radical generation on silica-supported TiO_2 photocatalysts, Applied Catalysis B 62 (3–4) (2006) 201–207.
[24] S.F. Chen, Y.Z. Liu, Study on the photocatalytic degradation of glyphosate by TiO_2 photocatalyst, Chemosphere 67 (5) (2007) 1010–1017.
[25] M.M. Mohamed, M.M. Al-Esaimi, Characterization, adsorption and photocatalytic activity of vanadium-doped TiO_2 and sulfated TiO_2 (rutile) catalysts: degradation of methylene blue dye, Journal of Molecular Catalysis A: Chemical 255 (1–2) (2006) 53–61.
[26] P. Mohapatra, K.M. Parida, Photocatalytic activity of sulfate modified titania 3: decolorization of methylene blue in aqueous solution, Journal of Molecular Catalysis A-Chemical 258 (1–2) (2006) 118–123.
[27] Y.J. Jang, C. Simer, T. Ohm, Comparison of zinc oxide nanoparticles and its nano-crystalline particles on the photocatalytic degradation of methylene blue, Materials Research Bulletin 41 (1) (2006) 67–77.
[28] H. Lachheb, E. Puzenat, A. Houas, M. Ksibi, E. Elaloui, C. Guilard, J.M. Herrmann, Photocatalytic degradation of various types of dyes (Alizarin S, Crocein Orange G, Methyl Red, Congo Red, Methylene Blue) in water by UV-irradiated titania, Applied Catalysis B 39 (2002) 75–90.
[29] T.Y. Zhang, T. Oyama, A. Aoshima, H. Hidaka, J.C. Zhao, N. Serpone, Photooxidative N-demethylation of methylene blue in aqueous TiO_2 dispersions under UV irradiation, Journal of Photochemistry and Photobiology A: Chemistry 140 (2001) 163–172.
[30] A. Houas, H. Lachheb, M. Ksibi, E. Elaloui, C. Guillard, J.M. Herrmann, Photocatalytic degradation pathway of methylene blue in water, Applied Catalysis B: Environmental 31 (2001) 145–157.
[31] R. Asahi, T. Morikawa, T. Ohwaki, K. Aoki, Y. Taga, Visible-light photocatalysis in nitrogen-doped titanium oxides, Science 293 (2001) 269–271.
[32] Y. Yang, Q.Y. Wu, Y.H. Guo, C.W. Hu, E.B. Wang, Efficient degradation of dye pollutants on nanoporous polyoxotungstate–anatase composite under visible-light irradiation, Journal of Molecular Catalysis A: Chemical 225 (2) (2005) 203–212.
[33] Q. Wang, C.C. Chen, D. Zhao, W.H. Ma, J.C. Zhao, Change of adsorption modes of dyes on fluorinated TiO_2 and its effect on photocatalytic degradation of dyes under visible irradiation, Langmuir 24 (2008) 7338–7345.
[34] J. Marugán, D. Hufschmidt, G. Sagawe, V. Selzer, D. Bahnemann, Optical density and photonic efficiency of silica-supported TiO_2 photocatalysts, Water Research 40 (2006) 833–839.
[35] S. Sakthivel, M.V. Shankar, M. Palanichamy, B. Arabindoo, D.W. Bahnemann, V. Murugesan, Enhancement of photocatalytic activity by metal deposition: characterisation and photonic efficiency of Pt, Au and Pd deposited on TiO_2 catalyst, Water Research 38 (2004) 3001–3008.
[36] A. Kudo, Development of photocatalyst materials for water splitting, International Journal of Hydrogen Energy 31 (2) (2006) 197–202.
[37] F. Izumi, A software package for the Rietveld analysis of x-ray and neutron diffraction patterns, Journal of Crystallography Association of Japan 27 (1985) 23–26.
[38] J. Tauc, R. Grigorovici, A. Vancu, Optical properties and electronic structure of amorphous germanium, Physica Status Solidi (b) 15 (1966) 627–637.
[39] M.A. Butler, Photoelectrolysis and physical properties of the semiconducting electrode WO_2, Journal of Applied Physics 48 (5) (1977) 1914–1920.
[40] G. Liu, T. Wu, J. Zhao, H. Hidaka, N. Serpone, Photoassisted degradation of dye pollutants. 8. Irreversible degradation of alizarin red under visible light radiation in air-equilibrated aqueous TiO_2 dispersions, Environmental Science & Technology 33 (1999) 2081–2087.
[41] M. Wiegel, W. Middel, G. Blasse, Influence of ns^2 ions on the luminescence of niobates and tantalates, Journal of Materials Chemistry 5 (7) (1995) 981–984.
[42] M. Oshikiri, M. Boero, J.H. Ye, Z.G. Zou, G. Kido, Electronic structures of promising photocatalysts $InMO_4$ (M = V, Nb, Ta) and $BiVO_4$ for water decomposition in the visible wavelength region, Journal of Chemical Physics 117 (2002) 7313–7318.